

Emulsion Chamber with Big Radiation Length for Detecting Neutrino Oscillations

A.E. Asratyan*, G.V. Davidenko, A.G. Dolgolenko, V.S. Kaftanov,
M.A. Kubantsev[†] and V.S. Verebryusov

Institute of Theoretical and Experimental Physics, Moscow, 117259 Russia

November 14, 2018

Abstract

A conceptual scheme of a hybrid-emulsion spectrometer for investigating various channels of neutrino oscillations is proposed. The design emphasizes detection of τ leptons by detached vertices, reliable identification of electrons, and good spectrometry for all charged particles and photons. A distributed target is formed by layers of low- Z material, emulsion-plastic-emulsion sheets, and air gaps in which τ decays are detected. The tracks of charged secondaries,

*Corresponding author. Tel.: (095)-237 0079. E-mail address asratyan@vxitep.itep.ru.

[†]Now at Kansas State University, Manhattan

including electrons, are momentum-analyzed by curvature in magnetic field using hits in successive thin layers of emulsion. The τ leptons are efficiently detected in all major decay channels, including $\tau^- \rightarrow e^- \nu \bar{\nu}$. Performance of a model spectrometer, that contains 3 tons of nuclear emulsion and 20 tons of passive material, is estimated for different experimental environments. When irradiated by the ν_μ beam of a proton accelerator over a medium baseline of $\langle L/E_\nu \rangle \sim 1$ km/GeV, the spectrometer will efficiently detect either the $\nu_\mu \rightarrow \nu_\tau$ and $\nu_\mu \rightarrow \nu_e$ transitions in the mass-difference region of $\Delta m^2 \sim 1$ eV², as suggested by the results of LSND. When exposed to the neutrino beam of a muon storage ring over a long baseline of $\langle L/E_\nu \rangle \sim 10$ –20 km/GeV, the model detector will efficiently probe the entire pattern of neutrino oscillations in the region $\Delta m^2 \sim 10^{-2}$ – 10^{-3} eV², as suggested by the data on atmospheric neutrinos.

PACS numbers: 14.60.Pq, 14.60.Fg

Keywords: neutrino oscillations, τ leptons, nuclear emulsion

1 Introduction

Oscillatory transitions among neutrinos of different flavors have emerged as a major topic of particle physics [1]. An accelerator experiment using muon antineutrinos from μ^+ decays at rest over an effective baseline of $L/E \sim 1$ m/MeV, LSND at Los Alamos, has reported a positive signal in the channel $\bar{\nu}_\mu \rightarrow \bar{\nu}_e$ with a probability of $\sim 3 \times 10^{-3}$ [2]. A consistent, albeit less significant, signal was also observed in the CP-conjugate channel $\nu_\mu \rightarrow \nu_e$ using muon neutrinos from π^+ decay in flight [3]. When combined with the upper limits imposed by other accelerator and reactor experiments [4, 5], the LSND data suggest that the $\bar{\nu}_\mu \rightarrow \bar{\nu}_e$ oscillation is driven by a mass difference squared, Δm^2 , between some 0.3 and 2.3 eV². The transitions $\bar{\nu}_\mu \rightarrow \bar{\nu}_e$ and $\nu_\mu \rightarrow \nu_e$ in this region of Δm^2 will soon be explored with higher sensitivity by the BooNE experiment at Fermilab [6].

Qualitatively, an analogy with the quark sector suggests that (i) the ν_τ should pick the largest contribution of the heaviest mass state ν_3 , and that (ii) the mixings between the neighboring neutrino flavors (*i.e.*, $\nu_e \leftrightarrow \nu_\mu$ and $\nu_\mu \leftrightarrow \nu_\tau$) should be the strongest. Therefore, a mass difference as large as $\Delta m^2 \sim 1$ eV² should primarily manifest itself in the $\nu_\mu \rightarrow \nu_\tau$ channel. The existing upper limits on the effective mixing $\sin^2 2\theta$ for the transition $\nu_\mu \rightarrow \nu_\tau$ [7, 8, 9] largely come from experiments with small effective baselines of $\langle L/E_\nu \rangle \ll 1$ km/GeV, and therefore are much less compelling for $\Delta m^2 \sim 1$ eV² than for larger values of the mass difference.

At neutrino energies well below the τ threshold ($E_\nu < 2$ GeV), the transition

$\nu_\mu \rightarrow \nu_\tau$ in the required region $\langle L/E_\nu \rangle \sim 1$ km/GeV will be indirectly probed by BooNE through ν_μ disappearance [6]. However, a convincing $\nu_\mu \rightarrow \nu_\tau$ signal can only be demonstrated by detecting the CC collisions of the ν_τ in appearance mode. For this, an appropriate environment is offered by the "medium-baseline" location on Mount Jura [10] in the ν_μ beam of CERN-SPS ($L = 17$ km and $\langle E_\nu \rangle = 27$ GeV by flux). The CC collisions of the ν_τ may be identified either topologically [10, 11] or by detecting the detached vertex of the produced τ in a hybrid-emulsion spectrometer [8]. The latter option is considered in this paper. For the "original" transition $\nu_\mu \rightarrow \nu_e$ to be observed and investigated in the same experiment, that will have very different systematics compared to either LSND [2] and BooNE [6], secondary electrons must be efficiently detected and momentum-analyzed.

The atmospheric evidence for neutrino oscillations driven by a mass difference of 10^{-2} – 10^{-3} eV² [12] will be initially probed by the long-baseline experiments operating in the neutrino beams of proton accelerators [13, 14, 10]. Large angular divergences of these beams dictate that, for the sake of statistics, fine instrumentation of the detector and/or the magnetic analysis be compromised for a multi-kiloton fiducial mass. Therefore, unraveling the pattern of oscillations in this mass region will probably require a much more intense beam generated by a muon storage ring with a straight section that points towards the detector [15]. Assuming a μ^- ring, the beam fully consists of muon neutrinos and electron antineutrinos whose energy spectra and angular spreads are precisely known. That the original beam contains

neither $\bar{\nu}_\mu$ nor ν_e allows to identify the parent neutrino by the sign of the lepton produced by the oscillated neutrino: negative and positive leptons are unambiguous signatures of the ν_μ and $\bar{\nu}_e$ parents, respectively. Therefore, the transitions $\nu_\mu \rightarrow \nu_e$, $\nu_\mu \rightarrow \nu_\tau$, $\bar{\nu}_e \rightarrow \bar{\nu}_\mu$, and $\bar{\nu}_e \rightarrow \bar{\nu}_\tau$ can be tagged independently.

The unique properties of this neutrino beam may warrant a finely instrumented detector of relatively small mass, that would be sensitive to a broad range of neutrino transitions driven by a mass difference of 10^{-2} – 10^{-3} eV². For this, several conditions are obligatory. Selecting the ν_τ and $\bar{\nu}_\tau$ collisions by the detached vertex of the τ is only possible in a hybrid-emulsion apparatus. In order to suppress the background to τ decays arising from anticharm production in CC collisions of the $\bar{\nu}_e$, the detector should identify the electrons as reliably as the muons. For the transitions $\nu_\mu \rightarrow \nu_\tau$ and $\bar{\nu}_e \rightarrow \bar{\nu}_\tau$ to be reliably discriminated, all charged secondaries (and not just muons) should be sign-selected and momentum-analyzed in the detector. The latter will also allow extra kinematic handles for further suppressing the background to τ decays (such as p_T of a decay particle with respect to τ direction and transverse disbalance of the event as a whole with respect to incident neutrino).

In this paper, we propose a conceptual scheme of a hybrid-emulsion spectrometer for detecting and identifying the neutrinos of different flavors by their CC collisions, as required for probing various channels of neutrino oscillations. The design emphasizes detection of τ leptons by detached vertices, reliable identification and sign-selection of electrons, good spectrometry for all charged secondaries,

and reconstruction of secondary photons and π^0 mesons. We also estimate the performance of the proposed apparatus in a medium-baseline experiment using the neutrino beam of the proton machine CERN-SPS and in a long-baseline experiment in the neutrino beam of a muon storage ring.

2 The detector

Building on the ideas put forth by A. Ereditato, K. Niwa, and P. Strolin [16], we implement the principle of "emulsion cloud chamber": layers of thin emulsion are only used as a tracker for events occurring in passive material. But in contrast with [16], we aim at constructing a distributed target with low density and large radiation length [11], so that either muons, hadrons, and electrons can be momentum-analyzed by curvature inside the target itself. Accordingly, the target should largely consist of low- Z material like aluminum or carbon in the form of carbon-fiber composite. Apart from narrow gaps instrumented with drift chambers that provide an electronic "blueprint" of the event, the target is built as a compact homogeneous volume in ambient magnetic field. Owing to relatively weak multiple scattering in low- Z material, the successive layers of thin emulsion may act as an "emulsion spectrometer" for analyzing the momenta of charged secondaries by curvature in magnetic field. In untangling the topologies of neutrino events, the detector will operate very much like a bubble chamber. The proposed apparatus is therefore referred to as the Emulsion Bubble Chamber, or EBC.

Specified below is a tentative structure of the distributed target that has been assumed in our simulations of detector response. (The actual design, including the choice of low- Z material, must of course be carefully optimized for a particular experiment). The fine structure of the target is depicted in Fig. 1. The 6-mm-thick basic element of the structure is formed by a 1-mm plate of passive material, by an emulsion–plastic–emulsion sheet (referred to as the ES) with total thickness of 0.2 mm, and by a relatively large drift space of 4.8 mm in which τ decays are selected. In our tentative design, the passive plate is largely carbon (960 μm), but also includes a thin layer of denser substance (40 μm of copper) in order to boost the geometric acceptance. The ES is a 100- μm sheet of transparent plastic coated on both sides with 50- μm layers of emulsion. The medium formed by successive elements has mean density of $\rho = 0.49 \text{ g/cm}^3$ and effective radiation length of $X_0 = 52.6 \text{ cm}$. (These values of ρ and X_0 are very similar to those of a bubble chamber with neon-hydrogen filling [17].) Note that the element does not feature the second ES downstream of the gap, as originally foreseen in [16]: the idea is to detect the kink or the trident using track segments in the ESs of two successive elements, as allowed by relatively weak Coulomb scattering in low- Z material of the intervening passive plate.

On the technical side, the air gap can be created by thin and rigid "bristles" on the upstream face of the carbon-composite plate that has been manufactured in "brush-like" form. (This is only possible because we have just one ES per element.) The positions of the thin bristles will be tabulated, and secondary vertices that

match these positions will be dropped. Another technical option for the drift space is 5-mm-thick paper honeycomb.

For a τ that emerged from the passive plate and suffered a one-prong or a three-prong decay in the gap, the decay vertex can be reconstructed from the track segments in two successive ESs. As soon as the fitted secondary vertex lies within the intervening passive plate, the candidate event must be dropped because of the high background from reinteractions. In principle, a τ that decayed before reaching the gap can be detected by impact parameter, but this possibility is not considered here. By adding a thin layer of denser material (copper) downstream of low- Z material (carbon), we slightly compromise the radiation length for geometric acceptance: thereby, the fraction of τ leptons that reach the air gap is effectively increased. That the proportion of copper events is boosted by the geometric effect is illustrated by Fig. 2. Here and below, the spectrum of incident τ neutrinos is assumed to be proportional to the spectrum of muon neutrinos from CERN-SPS [11].

For the tracks to be found in emulsion at scanning stage, planes of electronic detectors must be inserted in the continuous structure formed by the basic elements. These detectors should allow a crude on-line reconstruction of the event as a whole, and therefore they must have sufficient spatial resolution, provide angular information, and be spaced by less than one radiation length X_0 . In our tentative design, a stack of 30 elements forms a "module" with total thickness of $0.34X_0$, and 4-cm-wide

gaps between adjacent modules are instrumented by multisampling drift chambers.

In a medium- or long-baseline experiment where the occupancy of ESs will be relatively low, the accuracy of "electronic" reconstruction should be sufficient for unambiguously finding an energetic track in emulsion. Therefore, one can scan back along a stiff track, starting from the downstream ES of the module in which the collision occurred. As soon as the layer of origin is reached, a few successive ESs of the nearby elements must be fully scanned over relatively small areas towards finding the stubs of all other tracks associated with the primary vertex. To refine the alignment of ESs, a sufficient number of stiff muon tracks must be fully reconstructed in emulsion. This first stage of emulsion scanning will yield a relatively small number of events featuring decay signatures (either a kink or a trident in the air gap just downstream of the primary vertex). The second stage will be to scan down all tracks emerging from the primary vertex and to find and measure the conversions of secondary photons in the distributed target. This will allow to analyze the momenta of the secondaries in the "emulsion spectrometer" and to identify electrons by change of curvature and by emission of brems.

We foresee that the scanning of emulsion will only start after the full period of detector exposure.

3 Spectrometry for charged particles and photons

The response of the EBC detector is simulated using GEANT. In fitting a track, we assume that each tracker traversed (either a ES or a drift chamber) provides two spatial points with resolutions of 2 and 150 μm , respectively. Because of multiple scattering, the fit is but marginally sensitive to increasing the spatial error in the ES from 2 up to 8 μm . A uniform magnetic field of 0.7 Tesla, that is normal with respect to beam direction, is assumed throughout. (Using a stronger field would boost the performance of the spectrometer, but may be impracticable for a big air-core magnet that will house a multiton EBC.)

When found in emulsion, the track of an electron can be identified by a variation of curvature due to energy losses in successive layers of the target. These losses must be accounted for in estimating the momentum by curvature in magnetic field. For this, we use a simple algorithm that should be treated as preliminary and is not fully realistic. Namely, we fit a restricted segment of the e^- track over which the actual loss of energy does not exceed 30%.

Additionally, this segment is required to cross no less than five ESs. We compute an "ideal trajectory" for a given value of electron momentum p_e , to which the observed trajectory is then fitted, using GEANT. In doing so, we switch off multiple scattering and radiation losses, but instead reduce the momentum "by hand" in each layer of the target by the same amount Δp that is treated as an empirical parameter. The value of Δp is selected so as to obtain (i) an unbiased

estimate of electron momentum ($\langle p_e^{\text{meas}}/p_e^{\text{true}} \rangle \sim 1$) and (ii) a reasonable value of χ^2 .

For definiteness, we use a Monte-Carlo template of electrons with $p_e > 1$ GeV originating from simulated decays $\tau^- \rightarrow e^- \nu \bar{\nu}$ (see further). For these electrons, the mean length of the selected track segment is close to 30 cm (see Fig. 3), which proves to be sufficient for analyzing the momentum in the "emulsion spectrometer" formed by successive ESs of the distributed target. Plotted in Fig. 4 is the ratio between the fitted and true momenta, $p_e^{\text{meas}}/p_e^{\text{true}}$, for the properly fitted electrons ($\chi^2 < 3$). The same ratio is then separately shown for two regions of electron momentum: $1 < p_e < 5$ GeV and $p_e > 5$ GeV. We estimate that of all electrons with $p_e > 1$ GeV, nearly 90% can be reliably detected, identified, and sign-selected (that is, reconstructed with $\chi^2 < 3$ and $\delta p_e/p_e < 0.40$). On average, the e^- momentum is measured to a precision of some 11%.

Treating the length of the track segment as a free parameter of the fit, which is a more realistic approach that is not attempted in this paper, will further improve the momentum resolution and boost the fraction of sign-selected electrons. Good spectrometry for electrons will allow EBC to detect and discriminate the CC collisions of electron neutrinos and antineutrinos and, at the same time, to select electronic decays of the τ almost as efficiently as the muonic ones. A comparison between the two leptonic modes will provide an important handle on self-consistency of any τ signal.

The spectrometry of muons and charged pions is much less affected by en-

ergy loss in matter, but for pions the momentum resolution is slightly degraded by hadronic reinteractions. For the pions with $p_\pi > 1$ GeV originating from the simulated decays $\tau^- \rightarrow \pi^- \nu$, Fig. 5 shows the ratio between the fitted and true momenta, $p_\pi^{\text{meas}}/p_\pi^{\text{true}}$. The mean uncertainty on pion momentum is seen to be close to 7%.

Neutral pions can be reconstructed from photon conversions in the distributed target. (Here, we assume that the potential length in the detector is much larger than $X_0 = 52.6$ cm.) In estimating the energy of a photon that has converted in the target, we count only those conversion electrons that have fired at least one drift chamber and, therefore, can be found in emulsion and then momentum-analyzed by curvature. We also assume that the primary vertex has already been fitted, so that the direction of the photon is precisely known. For illustration, we consider the π^0 mesons originating from the decay $\tau^- \rightarrow \pi^- \pi^0 \nu$. The measured invariant mass of the two detected photons from $\pi^0 \rightarrow \gamma\gamma$, as plotted in Fig. 6, shows a distinct π^0 signal. The actual size of the mass window for selecting the π^0 candidates will be dictated by the level of combinatorial background in a particular analysis; for purely illustrative purposes, we assume a mass window of $115 < m_{\gamma\gamma} < 155$ MeV. Thus estimated detection efficiency for π^0 mesons is close to 0.26.

4 Detecting the leptonic and semileptonic decays of the τ

For the τ leptons emitted in either the deep-inelastic and quasielastic $\nu_\tau N$ collisions, we generate the two leptonic decays, $\tau^- \rightarrow \mu^- \nu \bar{\nu}$ and $\tau^- \rightarrow e^- \nu \bar{\nu}$, and three semileptonic (quasi-)two-body decays: $\tau^- \rightarrow \pi^- \nu$, $\tau^- \rightarrow \pi^- \pi^0 \nu$ that is mediated by the resonance $\rho^- \rightarrow \pi^- \pi^0$, and $\tau^- \rightarrow \pi^- \pi^+ \pi^- \nu$ that is mediated by the resonance $a_1^- \rightarrow \pi^- \pi^+ \pi^-$. The threshold effect for τ production in neutrino–nucleon collisions and polarization of the τ , that affects the angular distribution of decay products in the τ frame, are accounted for. Further details on our τ generator can be found in [18].

For definiteness, we again assume that τ neutrinos incident on EBC have the same energy spectrum as muon neutrinos from CERN-SPS [11] ($\langle E_\nu \rangle = 27$ GeV by flux), and that the distributed target is magnetized by a uniform field of 0.7 Tesla that is perpendicular to beam direction. The decay products of the τ are propagated through the target and then reconstructed from hits in emulsion, as explained in the previous section. In estimating the detection efficiencies for different decay channels of the τ , we adopt the (quasi-realistic) selection criteria that are listed below.

- The τ must have decayed in the drift gap. This is necessary for reconstructing the detached vertex from track segments in the upstream and downstream ESs.

- The momentum of either charged daughter must exceed 1 GeV, and its emission angle must lie within 400 mrad of beam direction. These selections are suggested by the fact that soft and broad-angle tracks are poorly reconstructed in emulsion.
- For a one-prong decay to a charged daughter d (either a muon, electron, or pion), the kink angle must be sufficiently large: $\theta_{\tau d} > 20$ mrad. This lower cut reflects the experimental uncertainty on the kink angle that is close to 5 mrad.
- All charged daughters of the τ must be momentum-analyzed by curvature and reliably sign-selected (that is, reconstructed in the detector with $\chi^2 < 3$ and $\delta p/p < 0.40$). This will fix the sign of the τ and, on the other hand, will allow kinematic handles for rejecting the decays of charmed and strange particles.
- In a one-prong decay, p_T of the charged daughter with respect to τ direction must exceed 250 MeV. This is aimed at rejecting the decays of strange particles.

For those τ decay channels that have actually been simulated in the detector, the estimated detection efficiencies (or acceptances) are listed in Table 1. (Note that here we do not require the π^0 from $\tau^- \rightarrow \pi^- \pi^0 \nu$ to be reconstructed.) For these decay channels of the τ , the acceptance-weighted branching fractions add up to some 0.28. Approximately accounting for the other one-prong and three-prong channels, we estimate that nearly 32% of all τ leptons produced in passive material will be detected in EBC by visible kinks or tridents.

The (quasi-)two-body decays $\tau^- \rightarrow \pi^- \nu$, $\tau^- \rightarrow \rho^- \nu$, and $\tau^- \rightarrow a_1^- \nu$ may provide an extra kinematic handle for discriminating the τ^- against the background of anticharm. In a decay $\tau^- \rightarrow h^- \nu$, "transverse mass" is defined as $M_T = \sqrt{m_h^2 + p_T^2} + p_T$, where m_h and p_T are the h^- mass and transverse momentum with respect to τ direction. The two-body kinematics dictate that the unsmeared M_T distribution should reveal a very distinctive peak just below $M_T^{\max} = m_\tau$, see the upper plots of Fig. 7. The M_T technique for identifying massive parents by two-body decays in emulsion was proven by discriminating the relatively rare decay $D_s^+(1968) \rightarrow \mu^+ \nu$ against a heavy background from other decays of charm [19]. Observing the high- M_T peak in a detector requires good spectrometry of charged pions and, for the decay $\tau^- \rightarrow \pi^- \pi^0 \nu$ in particular, good reconstruction of π^0 mesons. The bottom plots of Fig. 7 show the smeared M_T distributions for the reconstructed decays $\tau^- \rightarrow \pi^- \nu$, $\tau^- \rightarrow \pi^- \pi^0 \nu$, and $\tau^- \rightarrow \pi^- \pi^+ \pi^- \nu$ (the π^0 for $\tau^- \rightarrow \pi^- \pi^0 \nu$ has been selected in the mass window $115 < m_{\gamma\gamma} < 155$ MeV, see Fig. 6). The Jacobian cusps of the original M_T distributions largely survive the apparatus smearings of EBC and, therefore, will provide distinctive signatures of the τ .

5 Sensitivity to neutrino oscillations

Neutrino oscillations driven by $\Delta m^2 \sim 1$ eV [2] can be efficiently probed at a location on Mount Jura near CERN, that is irradiated by the existing wide-band ν_μ beam of the CERN-SPS accelerator ($\langle E_\nu \rangle = 27$ GeV by flux) over a "medium" baseline of 17

km [10]. At this location, an EBC detector can be deployed in the existing magnet of the NOMAD detector [11] that delivers a magnetic field of up to 0.7 Tesla. In the large internal volume of this magnet, $3.5 \times 3.5 \times 7.5 \text{ m}^3$, one might deploy a distributed target with a volume of $3.0 \times 3.0 \times 6.6 \text{ m}^3$, that will consist of 30 modules (see Section 2). The target has a total thickness of 10 radiation lengths, and contains nearly 20 tons of passive material and 3 tons of standard emulsion (or a lesser amount of diluted emulsion, that may be warranted by a relatively low occupancy at a medium-baseline location). The magnetic volume will also house a few drift chambers downstream of the target. As photon conversions and electrons will be efficiently detected in the distributed target, no extra electromagnetic calorimeter is foreseen. The design of the muon system is not discussed in this paper.

At the Jura location, the rate of ν_μ -induced CC collisions has been estimated [10] as 843 events per ton of target per 10^{19} protons delivered by CERN-SPS. Assuming 10^{20} delivered protons which corresponds to 3–4 years of operation, the proposed detector will collect nearly 1.7×10^5 CC events. Even if the probability of the $\nu_\mu \rightarrow \nu_\tau$ transition is as small as 0.3% [2], we will detect some 80 τ events with a negligibly small background from the decays of strange and anticharm particles. (This prediction assumes a τ detection efficiency of 32%, as estimated above for the same beam, and takes into account the threshold effect in τ production.) Alternatively, a zero signal will allow to exclude (at 90% C.L.) an area of the parameter plane $(\sin^2 2\theta_{\mu\tau}, \Delta m_{\mu\tau}^2)$ that is depicted in Fig. 8.

As demonstrated above, EBC will very efficiently identify, sign-select, and momentum-analyze prompt electrons from CC collisions of electron neutrinos and antineutrinos. The energy of incident ν_e ($\bar{\nu}_e$) will be estimated to better than 10%. If at the Jura site the transition $\nu_\mu \rightarrow \nu_e$ indeed occurs with a probability of some 0.003 as in LSND [2], in an exposure of 10^{20} protons on target we will detect and reconstruct some 460 $\nu_e N \rightarrow e^- X$ events due to oscillated neutrinos against a background of nearly 860 CC events due to the original ν_e component of the beam [10]. As the original ν_e component of the beam is substantially harder than the ν_μ component, a $\nu_\mu \rightarrow \nu_e$ signal will effectively reduce the mean energy of $\nu_e N \rightarrow e^- X$ events.

A very intense and collimated beam of a muon storage ring [15] will allow long-baseline experiments with relatively small but finely instrumented detectors. For purely illustrative purposes, we assume an EBC detector as sketched above (20 tons of passive material plus 3 tons of standard emulsion) that is irradiated by a μ^- ring with parameters as foreseen in [15] (that is, 7.5×10^{20} injected muons per year of operation and a straight section that amounts to 25% of the ring circumference). We also assume a "nominal" distance of 732 km (either from CERN to Gran Sasso or from Fermilab to Soudan) that results in effective baselines of $\langle L/E_\nu \rangle \sim 20$ and 10 km/GeV for the stored-muon energies of $E_\mu = 50$ and 100 GeV, respectively. Then, given unpolarized muons with $E_\mu = 50$ (100) GeV in the ring, in the absence of oscillations the detector will annually collect some 5.5×10^3 (4.4×10^4) and 2.4×10^3

(1.9×10^4) CC collisions of muon neutrinos and electron antineutrinos, respectively. Note that the expected event rate for $E_\mu = 100$ GeV is as high as in the CERN-SPS beam at Jura location.

Taken together, the data on atmospheric [12] and reactor [20] neutrinos favor a $\nu_\mu \rightarrow \nu_\tau$ transition with almost maximal mixing and with a mass difference in the range $\Delta m_{\mu\tau}^2 \sim 10^{-2}$ – 10^{-3} eV² [21, 22, 23]. For definiteness assuming $\sin^2 2\theta_{\mu\tau} = 1$ and $\Delta m_{\mu\tau}^2 = 5 \times 10^{-3}$ eV², we estimate that in three years of operation a 20-ton EBC will detect a signal of some 50 (170) τ^- leptons for $E_\mu = 50$ (100) GeV with a negligible background of $\bar{\nu}_e$ -produced anticharm. (Note that the E_μ -dependence of the τ signal largely reflects the increase of $\sigma(\nu_\tau N \rightarrow \tau^- X)$ with neutrino energy: in the region $\Delta m^2(\text{eV}^2) \ll \langle E_\nu \rangle / L$ (GeV/km), the flux of oscillated neutrinos is virtually independent of E_μ .) Alternatively, a zero τ^- signal will effectively exclude a large area of parameter space for the transition $\nu_\mu \rightarrow \nu_\tau$, see Fig. 8. The transition $\bar{\nu}_e \rightarrow \bar{\nu}_\tau$ will be simultaneously detected with a comparable sensitivity, and the two transitions will be reliably discriminated by the charge of the τ . Using the detached-vertex information, the transitions $\nu_\mu \rightarrow \nu_e$ and $\bar{\nu}_e \rightarrow \bar{\nu}_\mu$ will be separated from the transitions $\nu_\mu \rightarrow \nu_\tau$ and $\bar{\nu}_e \rightarrow \bar{\nu}_\tau$ involving the leptonic decays $\tau^- \rightarrow e^- \nu \bar{\nu}$ and $\tau^+ \rightarrow \mu^+ \nu \bar{\nu}$, respectively. We may conclude that, in this experimental environment, even a relatively small EBC detector will efficiently probe the entire pattern of neutrino oscillations in the region $\Delta m^2 \sim 10^{-2}$ – 10^{-3} eV².

6 Summary

A conceptual detector scheme is proposed for studying various channels of neutrino oscillations. The hybrid-emulsion spectrometer will detect and discriminate the neutrinos of different flavors by their CC collisions. The design emphasizes detection of τ leptons by detached vertices, identification and sign-selection of electrons, and spectrometry for all charged particles and photons. A distributed target is formed by layers of low- Z material, emulsion-plastic-emulsion sheets, and air gaps in which τ decays are detected. Target modules with mean density of 0.49 g/cm^3 and radiation length of 52.6 cm , that are similar to those of a bubble chamber with neon-hydrogen filling, are alternated by multisampling drift chambers that provide electronic tracking in real time. The tracks of charged secondaries, including electrons, are momentum-analyzed by curvature in magnetic field using hits in successive thin layers of emulsion and in drift chambers. Electrons are identified by change of curvature and by emission of brems. Photons are detected and analyzed by conversions in the distributed target, and neutral pions are reconstructed. The τ leptons are efficiently detected and sign-selected in all major decay channels, including $\tau^- \rightarrow e^- \nu \bar{\nu}$.

At a medium-baseline location on mount Jura in the existing neutrino beam of the proton machine CERN-SPS, the detector will be sensitive to either the $\nu_\mu \rightarrow \nu_\tau$ and $\nu_\mu \rightarrow \nu_e$ transitions in the mass-difference region of $\Delta m^2 \sim 1 \text{ eV}^2$, as suggested by the results of LSND. At a long-baseline location in the neutrino beam of a muon

storage ring, even a relatively small spectrometer of the proposed type will efficiently probe the entire pattern of neutrino oscillations in the region $\Delta m^2 \sim 10^{-2}-10^{-3} \text{ eV}^2$ that is suggested by the data on atmospheric neutrinos.

This work was supported in part by the CRDF foundation (grant RP2-127) and by the Russian Foundation for Fundamental Research (grant 98-02-17108).

References

- [1] K. Zuber, *On the Physics of Massive Neutrinos*, Physics Reports 305 (1998) 295;
J. Brunner, *Experimental Results on Neutrino Masses and Lepton Mixing*, preprint CERN-PPE/97-38, April 1997.
- [2] C. Athanassopoulos *et al.*, LSND Coll., Phys. Rev. Lett. 77 (1996) 3082.
- [3] C. Athanassopoulos *et al.*, LSND Coll., Phys. Rev. Lett. 81 (1998) 1774.
- [4] B. Achkar *et al.*, Bugey Coll., Nucl. Phys. B 434 (1995) 503.
- [5] L. Borodovsky *et al.*, E776 Coll., Phys. Rev. Lett. 68 (1992) 274.
- [6] E. Church *et al.*, BooNE Coll., *A Proposal for an Experiment to Measure $\nu_\mu \rightarrow \nu_e$ Oscillations and ν_μ Disappearance at the Fermilab Booster: BooNE*, December 7, 1997.
- [7] F. Dydak *et al.*, CDHS Coll., Phys. Lett. B 134 (1984) 281.
- [8] N. Ushida *et al.*, E531 Coll., Phys. Rev. Lett. 57 (1986) 2897.
- [9] E. Eskut *et al.*, CHORUS Coll., Phys. Lett. B 424 (1998) 202; preprint CERN-EP/98-73, May 1998;
P. Astier *et al.*, NOMAD Coll., Phys. Lett. B 431 (1998) 219; preprint CERN-EP/99-32, February 1999.

- [10] J.P. Revol *et al.*, ICARUS Coll., *A Search Program for Explicit Neutrino Oscillations at Long and Medium Baselines with ICARUS Detectors*, ICARUS-TM-97/01, March 1997.
- [11] J. Altegoer *et al.*, NOMAD Coll., Nucl. Instr. and Meth. A 404 (1998) 96.
- [12] Y. Fukuda *et al.*, Kamiokande Coll., Phys. Lett. B 335 (1994) 237; S. Hatakeyama *et al.*, Kamiokande Coll., Phys. Rev. Lett. 81 (1998) 2016;
Y. Fukuda *et al.*, Superkamiokande Coll., Phys. Rev. Lett. 81 (1998) 1562;
Phys. Lett. B 433 (1998) 9; Phys. Lett. B 436 (1998) 33;
M. Ambrosio *et al.*, MACRO Coll., Phys. Lett. B 434 (1998) 451.
- [13] Y. Oyama *et al.*, K2K Coll., preprint KEK 97-266, January 1998.
- [14] E. Ables *et al.*, MINOS Coll., Fermilab Proposal P875, February 1995; MINOS Coll., *The MINOS Detector Technical Design Report*, Fermilab report NuMI-L-337, October 1998.
- [15] S. Geer, in *Proc. Workshop on Physics at the First Muon Collider and at the Front End of a Muon Collider*, Fermilab, November 1997, published in AIP Conf. Proc. 435 (1998); Phys. Rev. D 57 (1998) 6989.
- [16] A. Ereditato, K. Niwa, and P. Strolin, preprint INFN/AE-97-06, Nagoya DAPNU-97-07, June 1997.
- [17] V.V. Ammosov *et al.*, E180 Coll., Nucl. Phys. B 177 (1981) 365;
K. Varvell *et al.*, WA59 Coll., Z. Phys. C 36 (1987) 1.

- [18] A. Asratyan *et al.*, Nucl. Instr. and Meth. A 427 (1999) 495.
- [19] K. Kodama *et al.*, E653 Coll., preprint DPNU-96-33, June 1996.
- [20] M. Apollonio *et al.*, CHOOZ Coll., Phys. Lett. B 420 (1998) 397.
- [21] M.C. Gonzalez-Garcia, H. Nunokawa, O.L.G. Perez, T. Stanev, and J.W.F. Valle, Phys. Rev. D 58 (1998) 033004.
- [22] O. Yasuda, Phys. Rev. D 58 (1998) 091301.
- [23] G.L. Fogli, E. Lisi, A. Marrone, and G. Scioscia, Phys. Rev. D 59 (1999) 033001.

Figure Captions

Fig. 1.

Schematic of the assumed fine structure of the target, showing the 1-mm-thick carbon-copper plates ($960 + 40 \mu\text{m}$), emulsion-plastic-emulsion sheets ($50 + 100 + 50 \mu\text{m}$), and drift space in which τ decays are selected ($4800 \mu\text{m}$).

Fig. 2.

The depth of the primary vertex in the carbon-copper plate for all τ events (a) and for those events in which the τ has decayed in the drift space (b). Here and in subsequent figures, the energy spectrum of incident τ neutrinos is assumed to be proportional to the spectrum of muon neutrinos from the CERN-SPS accelerator.

Fig. 3

The length along the beam direction of the track segment used for analyzing the e^- momentum by curvature (see text).

Fig. 4.

The ratio between the fitted and true momenta of the electron from $\tau^- \rightarrow e^- \nu \bar{\nu}$, $R = p_e^{\text{meas}}/p_e^{\text{true}}$, for $p_e > 1 \text{ GeV}$ (a), for $1 < p_e < 5 \text{ GeV}$ (b), and for $p_e > 5 \text{ GeV}$ (c).

Fig. 5.

The ratio between the fitted and true momenta, $R = p_\pi^{\text{meas}}/p_\pi^{\text{true}}$, for the π^- with $p_\pi > 1 \text{ GeV}$ originating from the decay $\tau^- \rightarrow \pi^- \nu$.

Fig. 6.

For the decay $\tau^- \rightarrow \pi^- \pi^0 \nu$ followed by $\pi^0 \rightarrow \gamma\gamma$, the measured invariant mass of the two photons that have been detected by conversions in the distributed target.

Fig. 7.

Transverse mass $M_T = \sqrt{m_h^2 + p_T^2} + p_T$ for the (quasi-)two-body decays $\tau^- \rightarrow h^- \nu$ with $h^- = \pi^-$ (left-hand column), $h^- = a_1^- \rightarrow \pi^- \pi^+ \pi^-$ (middle column), and $h^- = \rho^- \rightarrow \pi^- \pi^0$ (right-hand column). The unsmeared M_T distributions for all events in each channel prior to any selections are shown in the top row. The smeared distributions for detected events are shown in the bottom row.

Fig. 8.

Null-limit sensitivity to the $\nu_\mu \rightarrow \nu_\tau$ transition (at 90% C.L.) of a 20-ton EBC detector deployed at 17 km from CERN-SPS and at 732 km from a muon storage ring with $E_\mu = 50$ and 100 GeV, assuming 10^{20} protons delivered by CERN-SPS and 2.2×10^{21} negative muons injected in a ring with a straight section of 25%. The shaded area on the right is the region of parameter space for $\nu_\mu \rightarrow \nu_\tau$ suggested by a combined analysis of Kamiokande and Superkamiokande data [21]. Also illustrated are the best upper limits on $\sin^2 2\theta_{\mu\tau}$ for $\Delta m_{\mu\tau}^2 < 10 \text{ eV}^2$, as imposed by E531 [8] and CDHS [7].

Decay channel	Branching fraction	Acceptance	Acceptance times branching
$\tau^- \rightarrow \mu^- \nu \bar{\nu}$	0.174	0.40	0.070
$\tau^- \rightarrow e^- \nu \bar{\nu}$	0.178	0.36	0.064
$\tau^- \rightarrow \pi^- \nu$	0.113	0.40	0.045
$\tau^- \rightarrow \pi^- \pi^0 \nu$	0.252	0.30	0.076
$\tau^- \rightarrow \pi^- \pi^+ \pi^- \nu$	0.094	0.27	0.025

Table 1: The detection efficiencies, or acceptances, for those decay channels of the τ that have been simulated in the detector.

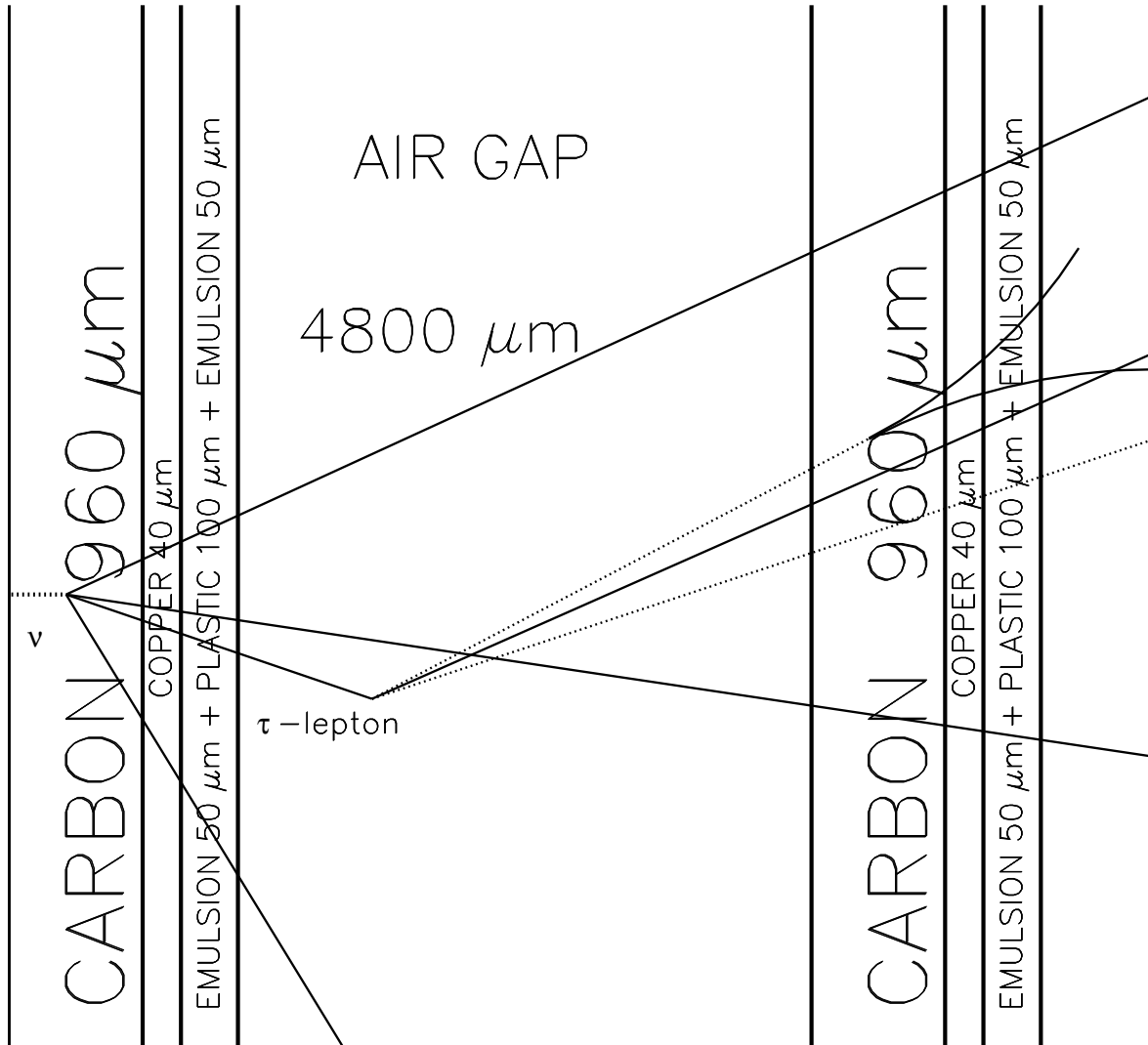


Figure 1: Schematic of the assumed fine structure of the target, showing the 1-mm-thick carbon-copper plates ($960 + 40 \mu\text{m}$), emulsion-plastic-emulsion sheets ($50 + 100 + 50 \mu\text{m}$), and drift space in which τ decays are selected ($4800 \mu\text{m}$).

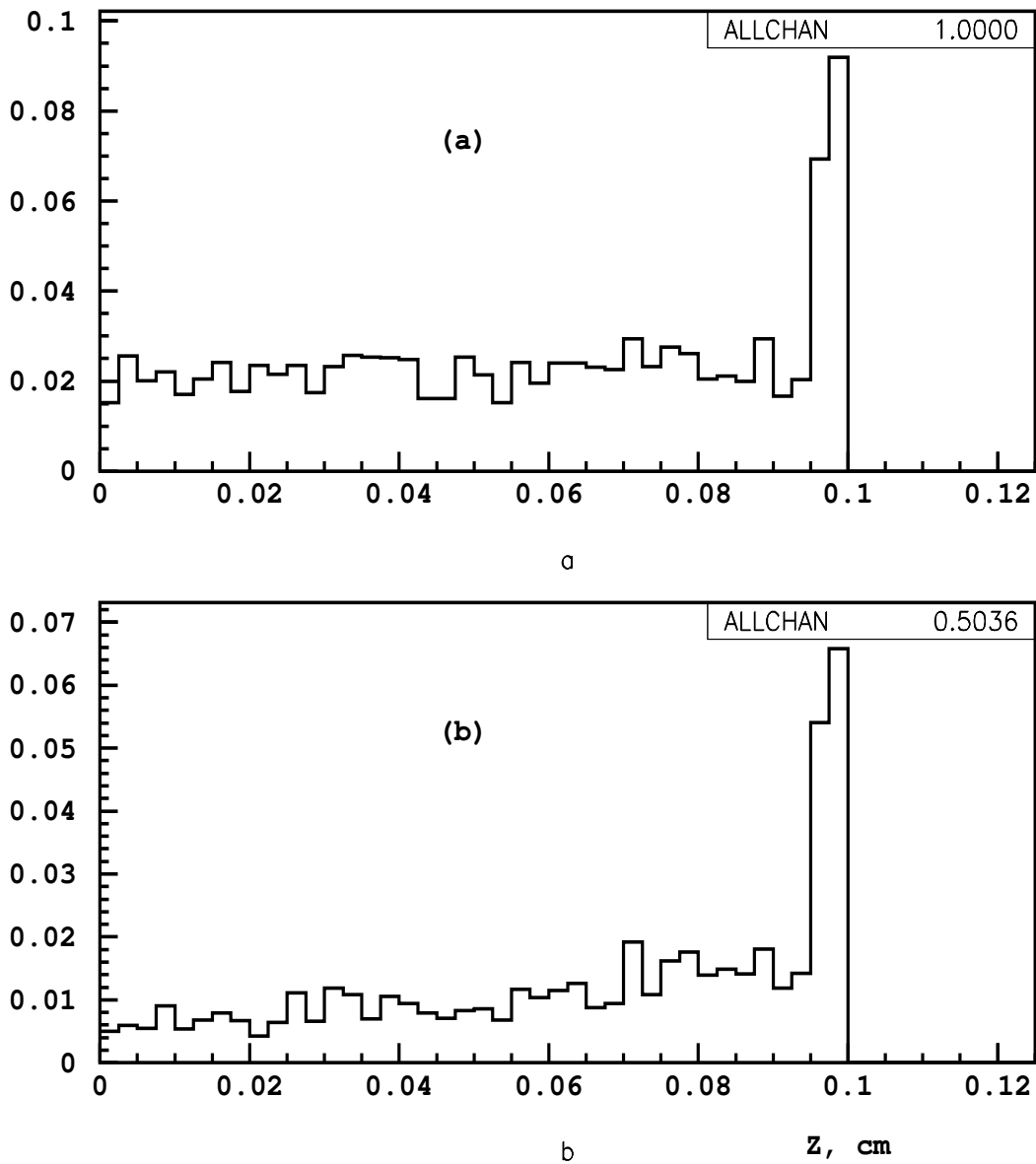


Figure 2: The depth of the primary vertex in the carbon-copper plate for all τ events (a) and for those events in which the τ has decayed in the drift space (b). Here and in subsequent figures, the energy spectrum of incident τ neutrinos is assumed to be proportional to the spectrum of muon neutrinos from the CERN-SPS accelerator.

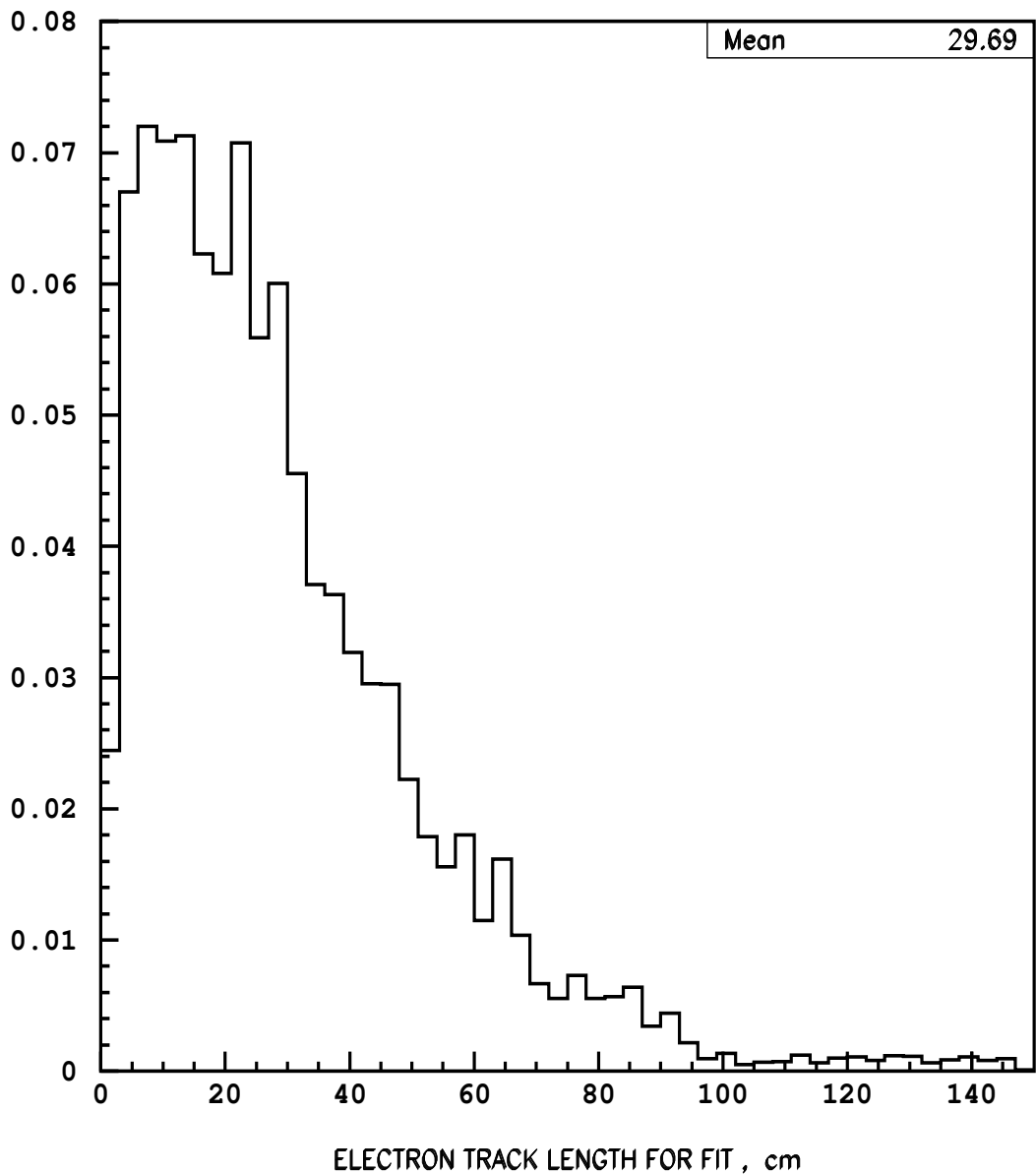


Figure 3: The length along the beam direction of the track segment used for analyzing the e^- momentum by curvature (see text).

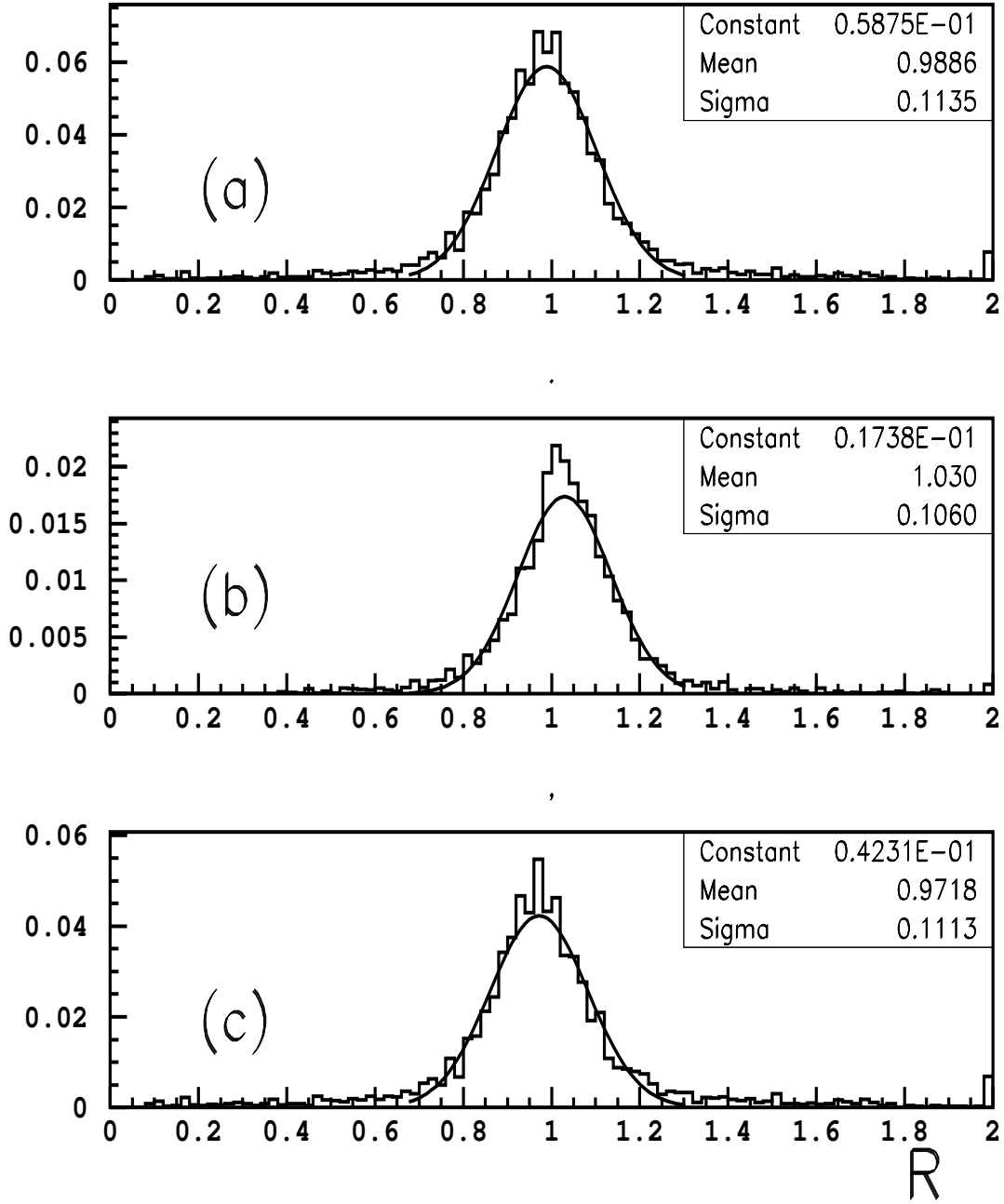


Figure 4: The ratio between the fitted and true momenta of the electron from $\tau^- \rightarrow e^- \nu \bar{\nu}$, $R = p_e^{\text{meas}} / p_e^{\text{true}}$, for $p_e > 1$ GeV (a), for $1 < p_e < 5$ GeV (b), and for $p_e > 5$ GeV (c).

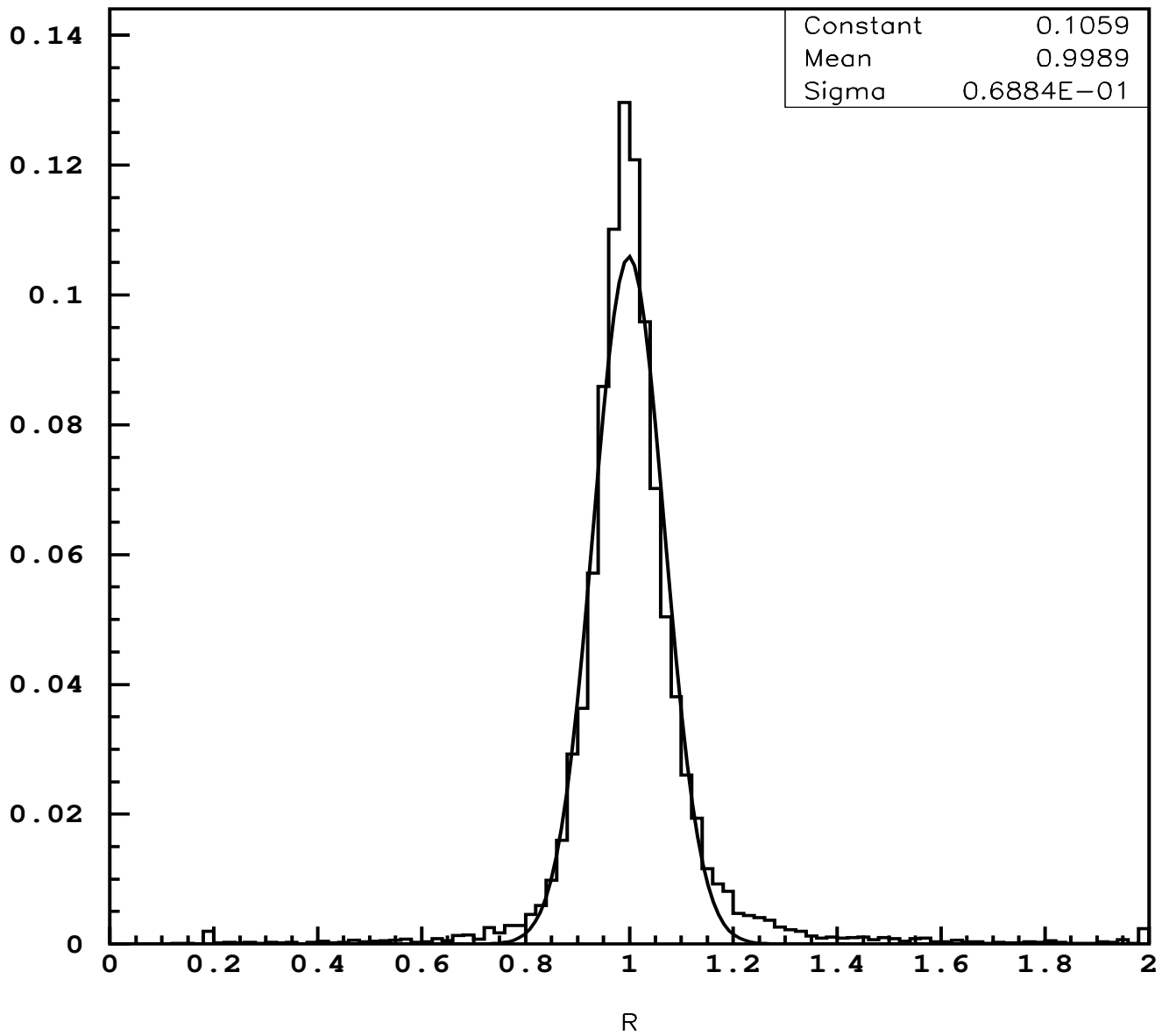


Figure 5: The ratio between the fitted and true momenta, $R = p_{\pi}^{\text{meas}}/p_{\pi}^{\text{true}}$, for the π^{-} with $p_{\pi} > 1$ GeV originating from the decay $\tau^{-} \rightarrow \pi^{-}\nu$.

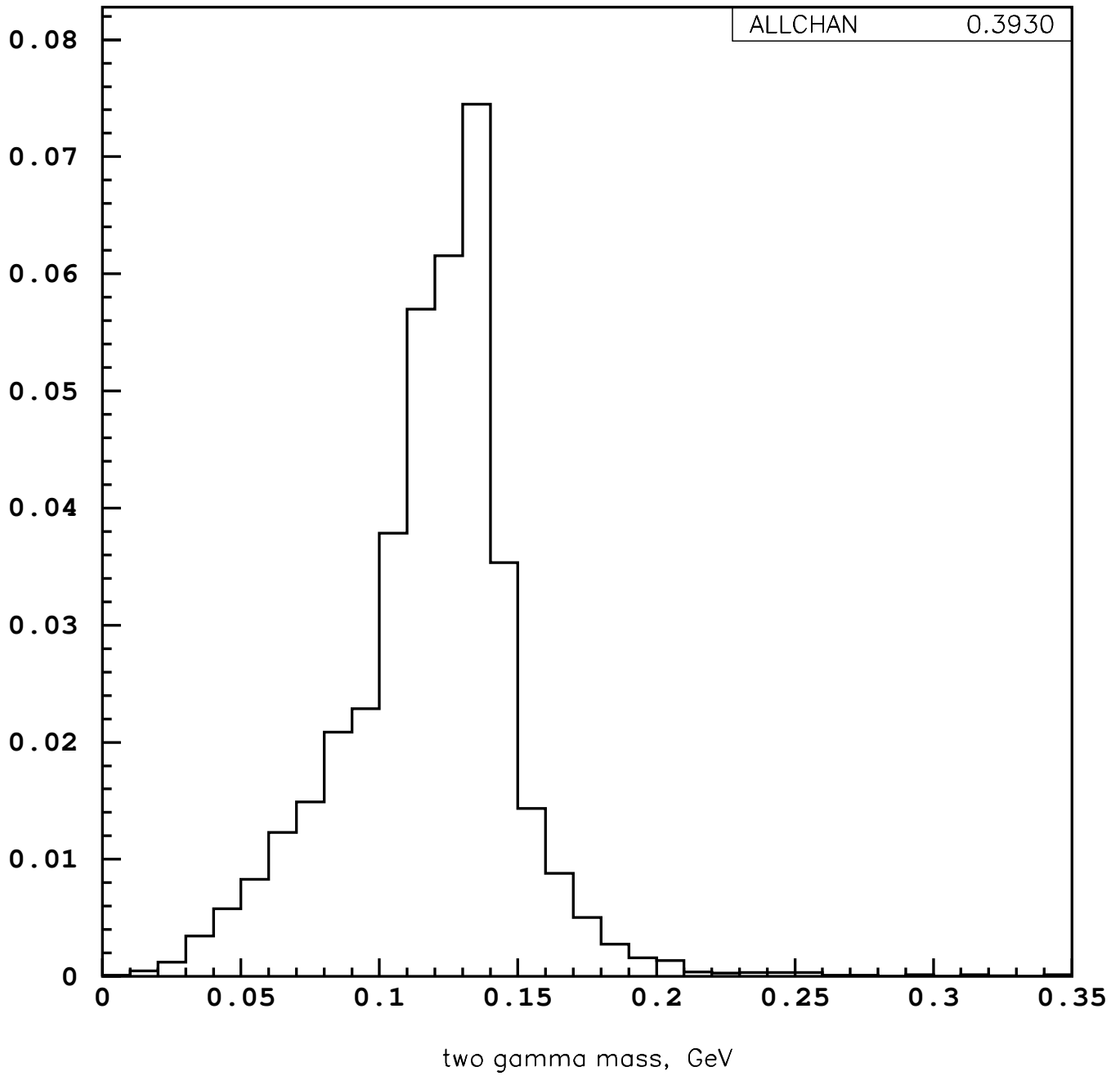


Figure 6: For the decay $\tau^- \rightarrow \pi^- \pi^0 \nu$ followed by $\pi^0 \rightarrow \gamma\gamma$, the measured invariant mass of the two photons that have been detected by conversions in the distributed target.

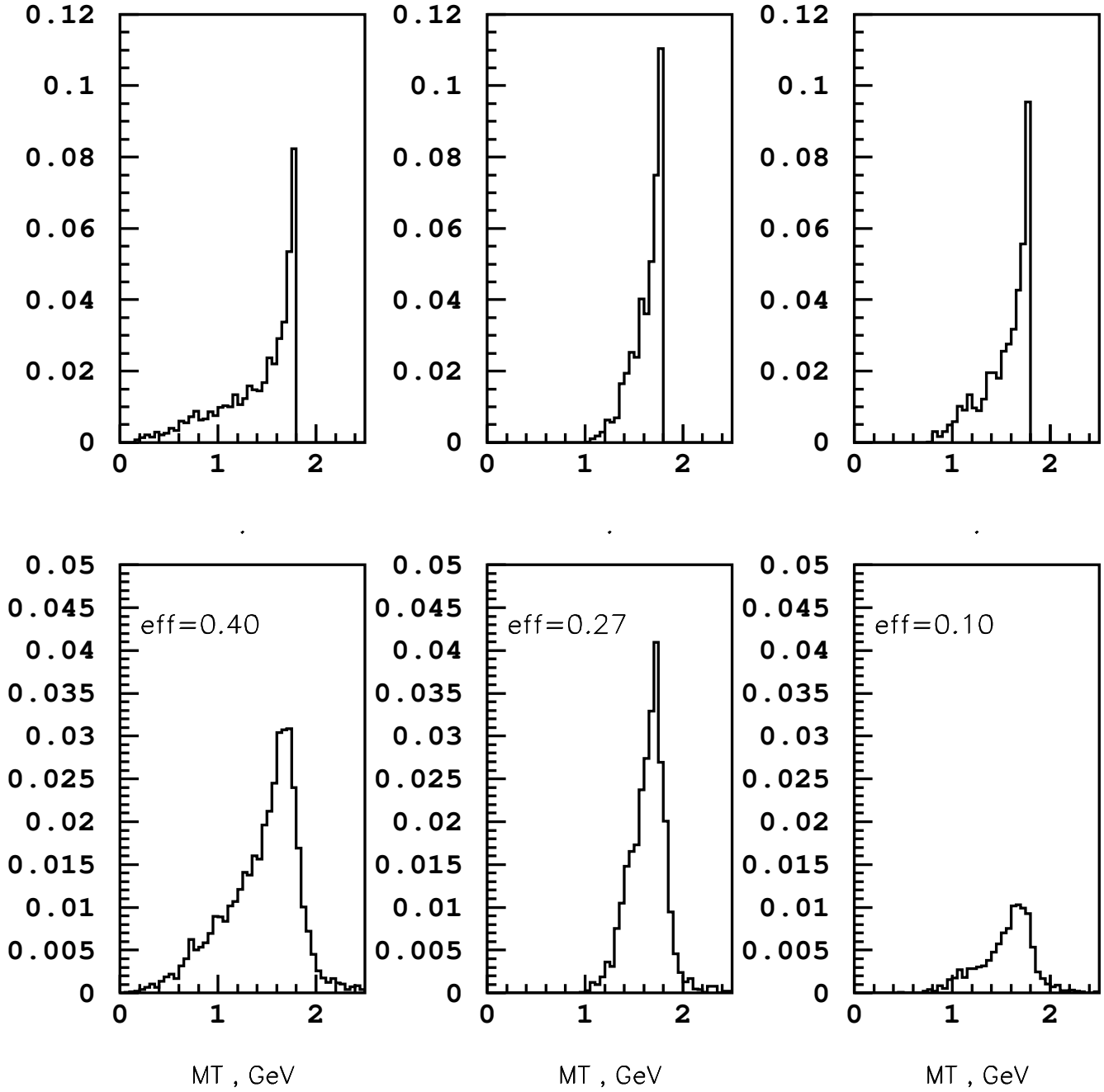


Figure 7: Transverse mass $M_T = \sqrt{m_h^2 + p_T^2} + p_T$ for the (quasi-)two-body decays $\tau^- \rightarrow h^- \nu$ with $h^- = \pi^-$ (left-hand column), $h^- = a_1^- \rightarrow \pi^- \pi^+ \pi^-$ (middle column), and $h^- = \rho^- \rightarrow \pi^- \pi^0$ (right-hand column). The unsmeared M_T distributions for all events in each channel prior to any selections are shown in the top row. The smeared distributions for detected events are shown in the bottom row.

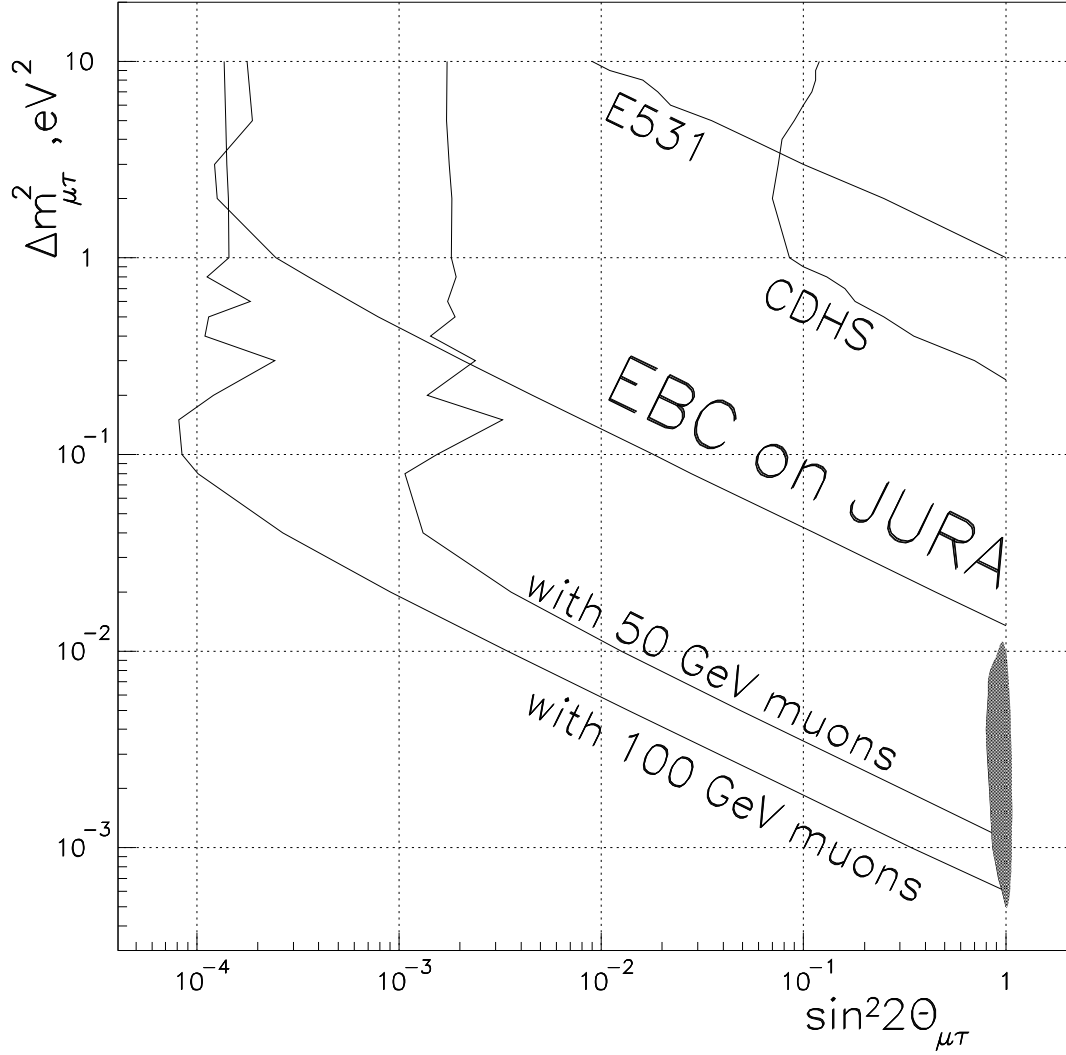


Figure 8: Null-limit sensitivity to the $\nu_\mu \rightarrow \nu_\tau$ transition (at 90% C.L.) of a 20-ton EBC detector deployed at 17 km from CERN-SPS and at 732 km from a muon storage ring with $E_\mu = 50$ and 100 GeV, assuming 10^{20} protons delivered by CERN-SPS and 2.2×10^{21} negative muons injected in a ring with a straight section of 25%. The shaded area on the right is the region of parameter space for $\nu_\mu \rightarrow \nu_\tau$ suggested by a combined analysis of Kamiokande and Superkamiokande data [21]. Also illustrated are the best upper limits on $\sin^2 2\theta_{\mu\tau}$ for $\Delta m_{\mu\tau}^2 < 10 \text{ eV}^2$, as imposed by E531 [8] and CDHS [7].